Article

Not peer-reviewed version

Structural investigation of the interaction between a GC-376 based peptidomimetic PROTAC and the viral main protease of Coxsackievirus B3 to explore the applicability of a broad-spectrum antiviral PROTAC

Alessia De Santis , Deborah Grifagni , Andrea Orsetti , Elena Lenci , Antonio Rosato , Mariapina D'Onofrio , Andrea Trabocchi , Simone Ciofi-Baffoni , Francesca Cantini * , Vito Calderone *

Posted Date: 17 July 2024

doi: 10.20944/preprints202407.1449.v1

Keywords: PROTAC; viral main protease; 3-Chymotrypsin-like protease; Coxsackievirus B3; SARS-CoV-2; GC-376

Article

Structural Investigation of the Interaction between a GC-376 Based Peptidomimetic PROTAC and the Viral Main Protease of Coxsackievirus B3 to Explore the Applicability of a Broad-Spectrum Antiviral PROTAC

Alessia De Santis [1,2], Deborah Grifagni [1,2], Andrea Orsetti [1,2], Elena Lenci [2], Antonio Rosato [1,2], Mariapina D' Onofrio [3], Andrea Trabocchi [2], Simone Ciofi-Baffoni [1,2], Francesca Cantini [1,2,*] and Vito Calderone [1,2,*]

[1] Magnetic Resonance Center CERM, University of Florence, Via Luigi Sacconi 6, 50019, Sesto Fiorentino, Florence, Italy; desantis@cerm.unifi.it (A.D.S.); grifagni@cerm.unifi.it (D.G.); a.orsetti@uu.nl (A.O.); rosato@cerm.unifi.it (A.R.); ciofi@cerm.unifi.it (S.C.-B.)

[2] Department of Chemistry, University of Florence, Via della Lastruccia 3, 50019, Sesto Fiorentino, Florence, Italy; elena.lenci@unifi.it (E.L.); andrea.trabocchi@unifi.it (A.T.)

[3] Department of Biotechnology, University of Verona, Strada le Grazie 15, 37134 Verona, Italy; mariapina.donofrio@univr.it

* Correspondence: cantini@cerm.unifi.it (F.C.); calerone@cerm.unifi.it (V.C.)

Abstract: The conservation of the main protease in viral genomes, combined with the absence of a homologous protease in humans, makes this enzyme family an ideal target for developing broad-spectrum antiviral drugs with minimal host toxicity. GC-376, a peptidomimetic 3CL protease inhibitor, has shown significant efficacy against coronaviruses. Recently, a GC-376-based PROTAC was developed to target and induce the proteosome-mediated degradation of the dimeric SARS-CoV-2 3CLPro protein. Extending this approach, the current study investigates the application of the GC-376 PROTAC to the 3CPro protease of Enteroviruses, specifically characterizing its interaction with CVB3 3CPro through X-ray crystallography, NMR and biophysical techniques. The present structural data show that there are some changes between the binding of CVB3 3CPro and SARS-CoV-2 3CLPro, but the overall similarity is strong. The most notable variation is the orientation of the phenylmethyl ester of GC-376 with the S4 subsite of the proteases. This is linked to the flexibility of the protein structure around the region of the catalytic triad shown by our NMR data. Other structural variations include distinct ligand interactions in subsites S1 and S2, influenced by the presence of Glu71 in CVB3 3CPro. Despite these differences, the GC-376 PROTAC fits well within the binding sites of both proteases, demonstrating its potential as a broad-spectrum antiviral agent.

Keywords: PROTAC; viral main protease; 3-Chymotrypsin-like protease; Coxsackievirus B3; SARS-CoV-2; GC-376

1. Introduction

The cell uses the ubiquitin-proteasome system to degrade unwanted or misfolded cellular proteins [1,2]. To do that, the system targets proteins for proteasomal-mediated destruction by polyubiquitinating them and this process involves the sequential action of the E1 ubiquitin-activating enzyme, the E2 ubiquitin-conjugating enzyme, and the E3 ubiquitin-protein ligase [3–6]. The E3 ligase is responsible for attaching multiple ubiquitin molecules to lysine residues at recognition sites in the protein to be degraded. This post-translational modification serves as a signal for proteolytic action by the 26S proteasome [7]. This cellular degradation system has been exploited by PROteolysis TArgeting Chimera (PROTAC) technology in order to modulate the cell levels of target proteins and it has proven highly effective in targeting proteins associated with cancer, leading to the initiation of clinical investigations for over a dozen drug candidates [8–10]. The utilization of the PROTAC

 doi:10.20944/preprints202407.1449.v1

technology as antiviral agent, although more limited, has recently grown. In last year, it received indeed a strong impetus with four works, including one from our group, that delineated the use of different PROTAC molecules against the 3-chymotrypsin-like protease of SARS-Cov2 (SARS-CoV-2 3CLPro, hereafter) [11–14]. In our previous study, we have synthesized a PROTAC bifunctional molecule conjugating the GC-376 inhibitor, able to recognize the active site of SARS-CoV-2 3CLPro, with the pomalidomide ligand, able to select Cereblon (CRBN) E3 ligase, through a piperazine-piperidine linker [12]. We showed that this PROTAC molecule is able to interact with SARS-CoV-2 3CLPro forming a reversible covalent bond between the Cβ carbon of the α,β-unsaturated amide moiety and the catalytic Cys145 sulfur atom of the target. Moreover, we observed that our PROTAC molecule reduces protein levels of SARS-CoV-2 3CLPro in cultured cells without affecting cell viability. This demonstrates that a peptidomimetic-based PROTAC approach can combat viral infections within the Coronavirus genera, which showed a high degree of structural similarity in the active site of their 3CLPro [15].

Proteases are also important for the replication of viruses other than Coronaviruses [16]. Among them, we have the proteases encoded by the 3C region of the enteroviruses genome (3CPro, hereafter), such as Coxsackievirus B3 (CVB3), EV-D68, EV-A71 and Coxsackievirus A16 [17–19]. All these enteroviral pathogens are part of the picornavirus family [20]. Infection with some of these viruses can lead to serious outcomes and cause clinical disease much more frequently than coronaviruses. As an example, infection with Coxsackievirus B3, a nonenveloped single-stranded (+) RNA enterovirus, is the most common reason for viral myocarditis and sudden cardiac death, within the enterovirus genus, with a very malicious disease pattern [21,22]. No effective therapeutic strategy for the prevention and treatment of these diseases is nowadays available and enterovirus disease has medical impact, with newborn infants and young children being at risk for septic-like disease, particularly during periods of high enterovirus prevalence [23]. The fact that all these virally encoded proteases from Coronaviruses and Enteroviruses perform essential functions in the viral replication cycle by cleaving both viral and host targets [24,25], as well as the fact that there is no known human protease with a specificity for Gln at the cleavage site of the substrate pushed towards the development of an commercially viable antiviral drug targeting both virus families [26]. This approach is made viable because coronaviral 3CLPro exhibit a high degree of structural similarity across 3CPro of the picornavirus family [16]. Crystal structures of 3CLPro from both alpha and beta Coronaviruses [27,28] revealed that two of the three domains of these enzymes together resemble the chymotrypsin-like fold of enteroviral 3CPro, but there is an additional α-helical domain that is involved in the dimerization of coronaviral proteases. This dimerization is essential for the catalytic activity of 3CLPro, whereas the enteroviral 3Cpro functions as a monomer [27]. Furthermore, the enteroviral 3CPro maintains a classical Cys···His···Glu/Asp catalytic triad, whereas the coronaviral 3CLPro only has a Cys···His dyad [27]. Nevertheless, the two types of proteases share common features, in particular their almost absolute requirement for Gln in the P1 position of the substrate and space for only small amino-acid residues such as Gly, Ala, or Ser in the P1′ position, indicating that the coronaviral 3CLPro and the enteroviral 3CPro can be a common target for the design of broad-spectrum antiviral compounds [27]. Indeed, broad-spectrum inhibitors of both 3CLPro and 3CPro have been largely documented in the literature [29–38], encouraging us to explore the capability of the PROTAC molecule designed by us against SARS-CoV-2 3CLPro to target also enteroviral 3CPro. In order to validate this hypothesis and to develop broad-spectrum antiviral PROTACs able to attack both 3CLPro and 3CPro-dependent viral infections, we have here structurally studied, by X-ray crystallography and solution NMR, the interaction of 3CPro from Coxsackievirus B3 (CVB3 3CPro, hereafter) with the peptidomimetic PROTAC molecule previously selected on SARS-CoV-2 3CLPro (GC-376 PROTAC) as well as with its precursor (GC-376 PROTAC precursor), i.e. a dipeptidyl protease ligand [12]. We have also compared the inhibitory activity of GC-376 PROTAC precursor against CVB3 3CPro with that obtained in the case of SARS-CoV-2 3CLPro enzyme.

 doi:10.20944/preprints202407.1449.v1

2. Materials and Methods

2.1. Expression and Purification of CVB3 3C^{Pro}

CVB3 3C^{Pro} was expressed and purified modifying Fili et al. protocol [39]. In detail, the pET-24a(+) plasmid encoding the CVB3 3C^{Pro} protein with an hexahistidine-coding sequence at the C-terminus was used to transform BL21(DE3)pLysS *E. coli* competent cells. A single colony from the transformation plate was picked to inoculate a 50 mL preculture in Luria-Bertani (LB) medium containing 50 mg mL^{-1} kanamycin and 35 mg mL^{-1} chloramphenicol. After overnight incubation at 37°C, 20 mL of the preculture was used to inoculate 1 L LB medium containing 50 mg mL^{-1} kanamycin and 35 mg mL^{-1} chloramphenicol. When an optical absorption of 0.6 (at a wavelength of 600 nm) was reached, 1 mM isopropyl b-d-1-thiogalactopyranoside (IPTG) was added to induce overexpression. The culture was then left overnight at 23°C and centrifuged at 5500 rpm for 20 min at 4°C. The resulting pellet was resuspended in 20 mL lysis buffer consisting of 50 mM Tris–HCl, 300 mM NaCl, 10 mM imidazole, 5% glycerol, 0.1% Triton-X pH 7.7. The cell suspension was lysed by one cycle of freezing (-80°C) and thawing (+10–15°C) and sonication upon the addition of 20 mL lysis buffer, 2mM DTT and lysozyme (0.15 mg ml^{-1}). The soluble cellular fraction was obtained by centrifugation at 4°C at 40,000 rpm for 35 min. Then, the supernatant containing soluble CVB3 3C^{Pro} was loaded for Immobilized Metal Affinity Chromatography (IMAC) purification by using HisTrap FF 5mL column which was previously equilibrated with 50 mM Tris-HCl, 300 mM NaCl, 30 mM imidazole, 1 mM DTT pH 7.7 as binding buffer. After lysate loading, the column was washed with 20 column volumes of the same buffer and elution was executed with 10 column volumes of 50 mM Tris-HCl, 300 mM NaCl, 500 mM imidazole, 1 mM DTT pH 7.7 buffer solution. Fractions containing the target protein were pooled and concentrated by Amicon Ultra 10 kDa reaching 3.5 mL volume. Subsequently, the protein solution was loaded onto Hi Load Superdex 16/600 200 pg column for Size Exclusion Chromatography (SEC). Isocratic elution was performed with 1.2 column volumes of 10 mM HEPES, 300 mM NaCl, 1 mM EDTA, 1 mM DTT, pH 7.5 buffer solution. The final protein yield resulted in 45 mg/L of culture. The purity of CVB3 3C^{Pro} was checked by SDS-PAGE analysis. The production of ^{15}N-labelled and ^{13}C,^{15}N-labelled CVB3 3C^{Pro} was performed by following the same protocol just switching to a standard M9-medium containing $(^{15}NH_4)_2SO_4$ (1.2 g/L) and ^{13}C-glucose (4 g/L) as sources of nitrogen and carbon, respectively.

2.2. Analytical Gel Filtration

The protein size of CVB3 3C^{Pro} was analyzed using analytical gel filtration (superdex 200 10/300 increase column; GE Healthcare) calibrated with gel filtration marker calibration kit, 6500-66000 Da. Purified samples in 25 mM MES, 150 mM NaCl, pH 6.5 buffer was loaded on the column pre-equilibrated 25 mM MES, 150 mM NaCl, pH 6.5 running buffer. Elution profiles were recorded at 280 nm with a flow rate of 0.75 mL/min. A standard curve of the logarithm of the molecular weight of the standards vs. the $K_{av}=(V_e-V_0)/(V_t-V_0)$ (V_e, elution volume; V_0, dead volume; V_t, total volume) was used to calculate apparent molecular mass of CVB3 3C^{Pro}.

2.3. Crystallization, Data Collection and Structure Solution

Crystals of CVB3 3C^{Pro} in complex with GC-376 PROTAC precursor were obtained through co-crystallization in sitting drop by adding an aliquot of 2 µL of reservoir buffer (0.1 M Tris-HCl, 0.2 M $MgCl_2$ and 26% PEG4000, pH 8.5) to 2 µL of protein solution (20 mM Tris-HCl, 150 mM NaCl, 1 mM EDTA, 1 mM DTT, pH 7.8) containing the ligand (2-3-fold concentration with respect to the protein and dissolved in 10% DMSO); trays were stored at 20° C. The protein concentration in the sample was 5 mg/mL.

The dataset was collected in-house, using a BRUKER D8 Venture diffractometer equipped with a PHOTON III detector, at 100 K; the crystal used for data collection were cryo-cooled using 25% ethylene glycol in the mother liquor. The GC-376 PROTAC adduct crystal has been refined at 1.9 Å resolution: it belongs to space group C2 with one molecule in the asymmetric unit, a solvent content

 doi:10.20944/preprints202407.1449.v1

of about 50%, and a mosaicity of 0.4-0.6°. The data were processed using the program XDS [40] reduced and scaled using XSCALE [40] and amplitudes were calculated using XSCALE [40]. The structure has been solved with the molecular replacement technique using the 7QUW structure as the template model. The successful orientation and translation of the molecule within the crystallographic unit cell was determined with MOLREP [41]. The refinement and water molecule fitting has been carried out using PHENIX [42], applying default TLS restraints. In between the refinement cycles, the model was subjected to manual rebuilding using COOT [43]. The quality of the refined structures was assessed using the program MOLPROBITY [44]. Data processing and refinement statistics for the GC-376 PROTAC adduct are shown in Table S1. Coordinates and structure factors have been deposited in the PDB under the accession code 8S6F.

2.4. NMR Spectroscopy

Conventional multidimensional NMR techniques based on 3D triple-resonance experiments [45] were performed on an AVANCE 500 spectrometer equipped with a cryogenically cooled probe to obtain backbone resonance assignment of CVB3 $3C^{Pro}$ with and without GC-376 PROTAC precursor at 308 K. The final NMR sample condition was 50 mM phosphate buffer at pH 6.0 containing 100 mM NaCl, 50 mM arginine, 50 mM glutamate, 1 mM DTT and 1 mM EDTA and 10% (v/v) D_2O. All NMR spectra were processed using the standard Bruker software (Topspin 4.2) and analyzed with CARA program.

In order to monitor the interaction between CVB3 $3C^{Pro}$ and GC-376 PROTAC or its precursor, we performed a NMR titration, based on the acquisition of ^{1}H-^{15}N HSQC experiments at 308 K on Bruker AVANCE 950 MHz, by adding aliquots (up to a maximum of 10 µL final added volume) of the small molecule (GC-376 PROTAC or its precursor) dissolved in d_3-acetonitrile to the NMR tube containing ^{15}N-labeled CVB3 $3C^{Pro}$ (0.2-0.3 mM) up to a 1:1 ratio. All NMR titration data were analyzed comparing the ^{1}H-^{15}N HSQC spectra recorded along the additions of the small molecule with that of the initial state as well as with ^{1}H-^{15}N HSQC blank spectra of ^{15}N-labeled CVB3 $3C^{Pro}$ recorded titrating the protein with the same aliquot of d_3-acetonitrile, in order to identify the chemical shift changes induced by the organic solvent. In such a way, following the chemical shift changes observed in the ^{1}H-^{15}N HSQC maps along each stepwise titration we were able to assign selectively the residues affected by protein-protein interaction. Signals showing chemical shift changes occurring on a slow exchange regime of the NMR time scale were considered to map the interaction surface on CVB3 $3C^{Pro}$ upon the binding with the small molecule. The observed chemical shift changes were calculated as backbone weighted average chemical shift differences, i.e. $\Delta\delta_{avg}(HN)$, i.e. $(((\Delta H)^2 + (\Delta N/5)^2)/2)^{1/2}$, where ΔH and ΔN are chemical shift differences for backbone amide ^{1}H and ^{15}N nuclei, respectively. The estimation of the chemical shift threshold value to define meaningful chemical shift differences was obtained by averaging $\Delta\delta_{avg}(HN)$ values plus one standard deviation (1σ), following the standard procedure used in NMR protein-protein interaction studies [46].

The backbone dynamic properties of CVB3 $3C^{Pro}$ have been sampled through ^{15}N relaxation measurements. NMR experiments for measuring ^{15}N longitudinal (R_1) and transverse (R_2) relaxation rates [47] and $[^{1}H]^{15}N$ heteronuclear NOE values [48] were recorded at 298 K at 500 MHz, using a protein concentration of 300 µM. A temperature dependence of the backbone NH chemical shifts in the ^{1}H-^{15}N HSQC spectra allowed us to obtain the backbone resonance assignment of CVB3 $3C^{Pro}$ at 298 K. ^{15}N R_1, ^{15}N R_2, and steady-state $[^{1}H]^{15}N$ NOEs were obtained with previously described pulse sequences, which employ gradient selection and sensitivity enhancement, as well as minimal water suppression. ^{15}N R_2 were measured with a refocusing time (τ_{CPMG}) of 450 µs with the Carr-Purcell-Meiboom-Gill (CPMG) sequence. In all experiments, the water signal was suppressed with "water flipback" scheme. ^{15}N R_1 and ^{15}N R_2 relaxation rates were obtained by fitting the cross-peak volumes (I), measured as a function of the relaxation delay, to a single-exponential decay as described in the literature [49]. Heteronuclear $[^{1}H]^{15}N$ NOE values were calculated as the ratio of peak volumes in spectra recorded with and without saturation. The analysis of the uncertainties of ^{15}N R_1 and ^{15}N R_2 relaxation rates is carried out by comparing the peak intensity on duplicated spectra having the same relaxation delay. Estimates of the molecular tumbling value under the chosen experimental

 doi:10.20944/preprints202407.1449.v1

conditions of magnetic field and temperature were obtained using the program HydroNMR following the standard procedure [50].

2.5. Enzyme Inhibition Kinetics Assay

The synthesized GC-376 PROTAC and its precursor were assayed through a fluorometric assay using the fluorogenic substrate Hilyte Fluor-488-ESATLQSGLRKAK-(QXL-520)-NH_2 (Anaspec). All of the measurements were performed in 96-well plates with a Fluostar Optima microplate reader (BMG Labtech, Ortenberg, Germany) analogously to what previously performed [12]. Excitation and emission wavelengths were 490 and 520 nm, respectively. All incubations were performed at 30 °C in 10 mM HEPES buffer containing 150 mL NaCl, 1 mM EDTA, 1mM DTT at pH=7.4. The inhibitors were preincubated with CVB3 $3C^{Pro}$ enzyme (59 nM) for 10 min at 30 °C before the reaction was started by the addition of the fluorogenic substrate (1 μM). The increase of fluorescence signal was monitored over 30 min (λ_{ex} = 490 nm, λ_{em} = 520 nm) at 30 °C. The percentages of inhibition for the tested molecules were determined through the equation $(1 - V_s/V_o) \times 100$, where vs. is the initial velocity in the presence of the inhibitor and V_o is the initial velocity of the uninhibited reaction. The IC_{50} values were obtained by dose-response measurements using an inhibitor range of concentrations 0.1 nM to 0.3 mM for GC-376 PROTAC and 0.01 nM to 0.1 mM for GC-376 PROTAC precursor. All the experiments were performed in triplicate, and data collected were analyzed using GraphPad 5.0 Software Package (GraphPad Prism, Inc., San Diego, CA).

3. Results

3.1. Crystal Structure of CVB3 $3C^{Pro}$ in Complex with GC-376 PROTAC Precursor

To characterize the interaction of CVB3 $3C^{Pro}$ with both GC-376 PROTAC and its precursor, the same compounds previously used by us with SARS-CoV-2 $3CL^{Pro}$ (Figure S1), we performed crystallization trials through both ligand-co-crystallization and -soaking strategies. Well-diffracting crystals were obtained only in the case of the GC-376 PROTAC precursor. This result differs from what obtained with SARS-CoV-2 $3CL^{Pro}$, whose well-diffracting crystals were obtained with both the GC-376 PROTAC precursor and the GC-376 PROTAC by soaking and co-crystallization, respectively. The crystal structure of CVB3 $3C^{Pro}$ in complex with the GC-376 PROTAC precursor was solved at 1.9 Å resolution, which provided atomic details of the CVB3 $3C^{Pro}$-ligand interactions (**Table S1**). The overall 3D structure clearly resembles that of the free protein (PDB IDs 2VB0 and 3ZYD) with a negligible RMSD computed on backbone atoms. Only local loop regions showed backbone RMSD values higher than average. The structure of CVB3-$3C^{pro}$ adopts a chymotrypsin protein fold. The N terminus starts with an α-helix of residues 1-14 and is followed by two topologically equivalent β-barrels comprising residues 15-77 and 100-173, which pack together to form a narrow groove for substrate binding. The catalytic triad of Cys147, His40, and Glu71 is located in the cleft between the two β-barrels.

Concerning the presence of the protease ligand, we observed that the electron density is well defined for all atoms (Figure 1A). The ligand has been refined at full occupancy and the B-factor values of the atoms that are visible in the electron density are in line with those of the neighboring protein atoms (Table S1). The most relevant feature is the binding mode of the ligand to the catalytic Cys147, which occurs via a covalent bond between C5 and the sulfur atom of Cys147. From the crystallographic point of view, this is supported by the fact that the bond length spontaneously refines to values around 1.8 Å, which is coherent with a C-S covalent bond. From the chemical point of view, it is known that the formation of a covalent (even reversible) bond between the unsaturated carbon and the sulfur atom is very likely [51,52]. Besides the covalent bond, other polar and non-polar interactions keep the protease ligand in place (Figure 1B). The protein atoms involved in direct hydrogen bond interactions with the ligand are namely the backbone oxygen of Thr142, one of the imidazole nitrogen atoms of His161, the backbone oxygen of Val162, the backbone nitrogen atom of Gly164 and the backbone nitrogen atom of Cys147. Several more residues are involved in hydrophobic interactions, and this is in agreement with the relatively non-polar nature of the ligand.

 doi:10.20944/preprints202407.1449.v1

Despite the difference in terms of primary structure, the cavity that hosts the ligand has a very similar shape with respect to SARS-CoV-2 3CL^{Pro} (Figure 1C); for this reason, the binding mode and interactions are similar to those in the 8OKB and 8OKC structures [12]. The only exception is the conformation of the phenyl ring of the phenylmethyl ester, which is basically flipped by 90°. This effect is due to a different structural arrangement of the C-terminal segment of CVB3 3C^{Pro} with respect to that of SARS-CoV-2 3CL^{Pro}, which makes the substrate cavity of CVB3 3C^{Pro} more open. The larger available volume allows the phenyl ring to rotate in a position that is structurally more congested in SARS-CoV-2 3CL^{Pro} structure (Figure 1C). This evidence also suggests that the ligand is versatile and is able to efficiently interact with different protein targets, provided of course a certain degree of structural similarity among them. The alpha helical region capping from the top the substrate cavity in SARS-CoV-2 3CL^{Pro}, which is absent in the CVB3 3C^{Pro}, does not determine a different orientation of the nearby Leu sidechain of the ligand in the two structures. These results support that an antiviral PROTAC molecule acting on both coronaviral and enteroviral proteases can be constructed starting from our dipeptidyl protease ligand.

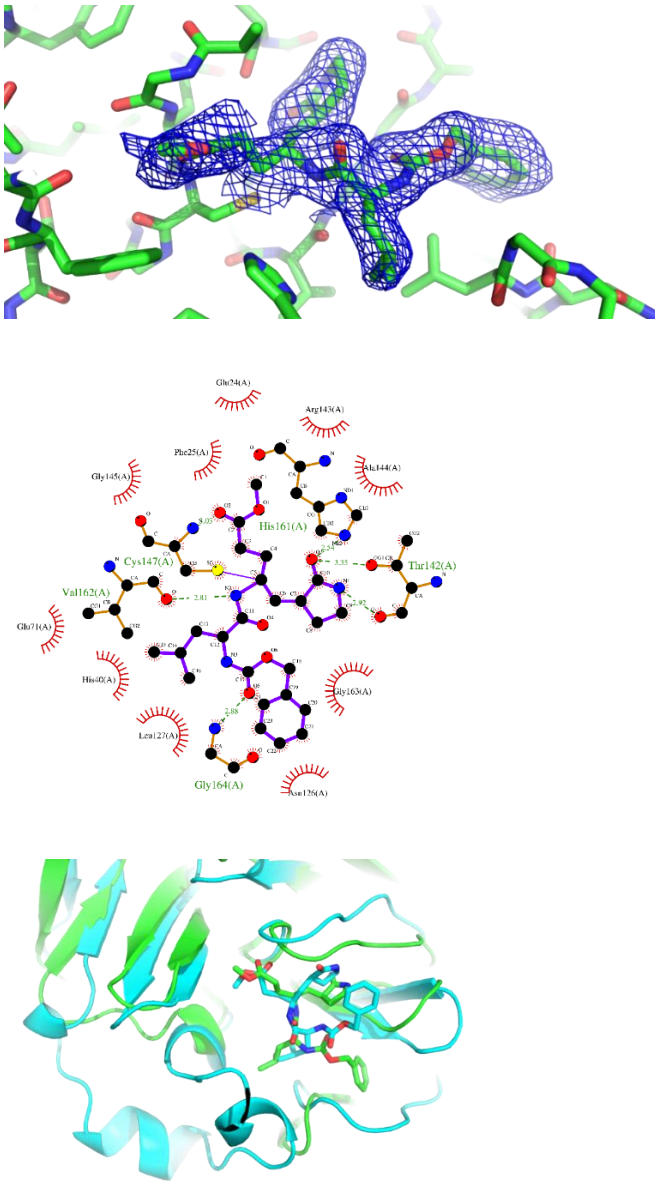

Figure 1. Crystal structure of CVB3 3CPro in complex with GC-376 PROTAC precursor. (**A**) 2Fo-Fc map of FT234 and Cys147 contoured at 0.9σ level. (**B**) Ligplot schematic view of binding mode of GC-376 PROTAC precursor. (**C**) Su-perposition of the binding cavity in CVB3 3CPro (green) and SARS-CoV-2 3CLPro (cyan) showing the similar orientation of the ligand in both structures.

 doi:10.20944/preprints202407.1449.v1

3.2. Structural characterization of CVB3 3C^{Pro} by solution NMR

Because of the failure to obtain crystals of GC-376 PROTAC-CVB3 3C^{Pro} complex, we decided to apply a solution NMR strategy to characterize the interaction between of GC-376 PROTAC and CVB3 3C^{Pro}. Since the backbone resonance assignment of CVB3 3C^{Pro} was not available, the first step was that to find the experimental sample conditions suitable to obtain 3D triple-resonance experiments that are necessary to extract the sequential information. The protein was produced in a ^{15}N and ^{13}C labelled medium and purified to a purity > 95% with two purification steps (Figure S2). Analytical gel filtration showed that the protein is homogenous with just one species present in solution corresponding to the monomeric form (Figure S2). The ^{1}H-^{15}N HSQC spectrum of CVB3 3C^{Pro} at 298 K in 50 mM phosphate buffer with 100 mM NaCl at pH 6.0 shows well-dispersed amide signals with few peaks clustered in the random-coil region (Figure S3). Nevertheless, the high quality of the ^{1}H-^{15}N HSQC spectrum is not reflected in 3D triple-resonance NMR experiments needed to achieve a complete backbone resonance assignment. Indeed, several NHs in the 3D triple-resonance NMR experiments lack the sequential pattern of signals required to unambiguously perform backbone resonance assignment. Moreover, in these conditions the protein has a strong tendency to precipitate over time in the NMR tube. Thus, to find suitable conditions to accomplish complete backbone resonance assignment, we performed a temperature dependence NMR analysis at different pHs and ionic strengths. As a result, we were able to improve the quality of the 3D triple-resonance experiments by using a 50 mM phosphate buffer at pH 6.0 containing 100 mM NaCl, 50 mM arginine, 50 mM glutamate, 1 mM DTT and 1 mM EDTA [53] and by acquiring the NMR spectra at 308 K. In these experimental conditions, the backbone amide NMR signals significantly narrowed and the number of the Cα and Cβ resonances are observed in the 3D spectra increased significantly. Thus, we could assign about 80% of the backbone NHs of CVB3 3C^{Pro}. In particular, we assigned all the cross-peaks detected in the ^{1}H-^{15}N HSQC spectrum, indicating that the unassigned backbone NHs are missing since they are very weak or broadened beyond detection. Mapping the latter NHs on the structure of CVB3 3C^{Pro}, we observed that they are located in a specific area involving the Cys···His···Glu residues of the catalytic triad and their surroundings (Figure 2A). This finding suggests that conformational motions on the µs-ms timescale occur in this region. To investigate more this aspect, we have measured ^{15}N longitudinal (R_1) and transverse (R_2) relaxation rates and [^{1}H]^{15}N heteronuclear NOE values of CVB3 3C^{Pro} (Figure S4). These data were used to obtain insights both into the motions of the backbone NHs at different time scales and to calculate, from the R_2/R_1 ratio, the overall correlation time for molecular tumbling (τ_m). In agreement with the results of the analytical gel filtration, the experimentally calculated τ_m value is 13.8 ± 1.9 ns, as expected for a protein of this size in a monomeric state and perfectly matching the τ_m value estimated by HYDRONMR [50] (13.7 ns) based on the monomeric crystal structure of CVB3 3C^{Pro} (PDB ID 3ZYD). The residues showing negative [^{1}H]^{15}N NOE values, indicating backbone motions on the ps-ns time scale, as well as those showing high R_2 over R_1 ratios, indicating backbone motions on the µs-ms timescale, were mapped on the structure of CVB3 3C^{Pro} (Figure 2A). These NHs are again located in the area involving the ligand-binding site. We can thus conclude that both broadening beyond detection effects as well as high internal flexibility from ps to ms timescale indicate that the backbone of the protein region of the catalytic triad is highly dynamic, thus preventing to perform a complete backbone resonance assignment. However, these findings suggested us that the addition of a ligand could dampen the highly dynamic properties of the ligand-binding site. To test this hypothesis, we have added one equivalent of the GC-376 PROTAC precursor to CVB3 3C^{Pro} and recorded a ^{1}H-^{15}N HSQC spectrum (Figure 2B) and a full set of the 3D triple-resonance experiments. It results that the quality of the 3D triple-resonance experiments is significantly improved (Figure 2C), in such a way allowing us to obtain a complete and accurate backbone resonance assignment at 308 K for the GC-376 PROTAC precursor-bound state of CVB3 3C^{Pro} (97% of assigned backbone NHs), with only five missing NHs (Met12, Lys20, Lys77, Gly156, Leu176). The backbone resonance assignment at 308 K has been deposited in the BioMagResBank (BMRB ID 52547).

 doi:10.20944/preprints202407.1449.v1

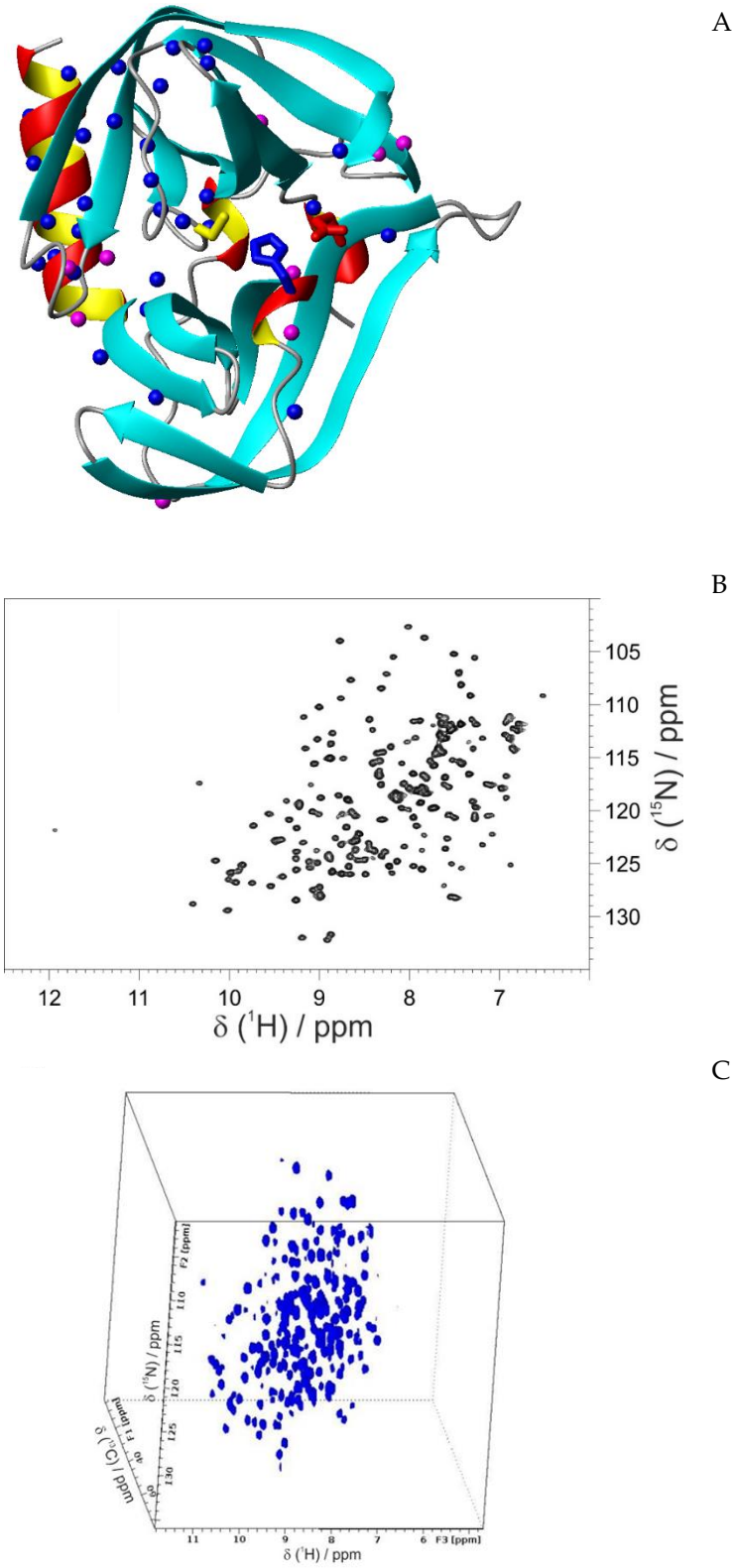

Figure 2. Structural-dynamic characterization of CVB3 $3C^{Pro}$ by solution NMR at 308K. (**A**) Backbone NHs broadened beyond detection and having high R_2/R_1 ratios are mapped in blue and magenta, respectively, on the crystal structure of CVB3 $3C^{Pro}$. The sidechains of the Cys···His···Glu residues of the catalytic triad are shown in yellow, blue and red, respectively. ^{1}H-^{15}N HSQC (**B**) and 3D CBCA(CO)NH (**C**) NMR spectra of CVB3 $3C^{Pro}$ acquired at 500 MHz and 308 K.

 doi:10.20944/preprints202407.1449.v1

3.3. Mapping the Interaction of GC-376 PROTAC and Its Precursor with CVB3 3C^{Pro} by Solution NMR

Thanks to having obtained the backbone resonance assignment of CVB3 3C^{Pro} with and without the GC-376 PROTAC precursor, we can identify the residues of CVB3 3C^{Pro} whose NH resonances are affected by the binding of the GC-376 PROTAC precursor as well as of GC-376 PROTAC. A NMR titration was first performed by adding stepwise the GC-376 PROTAC precursor to ^{15}N-labelled CVB3 3C^{Pro}. Several NH signals are affected by the GC-376 PROTAC precursor additions showing a slow exchange regime on the NMR time scale (Figures 3A and S5). Moreover, new NH signals appear with increasing intensities along the stepwise additions of GC-376 PROTAC precursor with their chemical shifts corresponding to those of the GC-376 PROTAC precursor-bound species (Figures 3A and S5). Taken together, these findings indicate that the GC-376 PROTAC precursor is tightly bound to CVB3 3C^{Pro}. Mapping both these type of NH changes on the crystal structure of CVB3 3C^{Pro} in complex with the GC-376 PROTAC precursor (Figure 3B), we can observe that the large majority of the backbone NHs surround the ligand. This indicates the specific binding of the precursor to the cavity containing the Cys···His···Glu/Asp catalytic triad. We then used the same approach to investigate the binding of GC-376 PROTAC: an NMR titration was thus performed by stepwise adding GC-376 PROTAC to ^{15}N-labelled CVB3 3C^{Pro}. The observed chemical shift changes essentially reproduce those occurring upon the precursor additions, with signals displaying a slow exchange regime on the NMR time scale and new signals appearing with increasing intensities along the titration. The comparison of the effects on the backbone chemical shifts of the binding of GC-376 PROTAC to ^{15}N-labelled CVB3 3C^{Pro} with respect to those generated by the GC-376 PROTAC precursor (Figure 4), showed that the position of essentially all of the corresponding signals fell within ±0.05 ppm. This demonstrates that the two molecules interact with CVB3 3C^{Pro} in a very similar mode. This data allows us to conclude that the linker and the pomalidomide ligand moiety are not tightly interacting with the protein surface thus displaying a high degree of mobility, similarly to what we have previously found upon the binding of the same GC-376 PROTAC molecule to SARS-CoV-2 3CL^{Pro}.

We evaluated the two ligands GC-376-PROTAC and its precursor for their ability to inhibit CVB3 3C^{Pro} through a fluorimetric enzyme inhibition kinetics assay using Hilyte Fluor-488-ESATLQSGLRKAK-(QXL-520)-NH$_2$ as the substrate. Both ligands showed an inhibition activity in the micromolar range, specifically displaying an IC$_{50}$ value of 14.8 μM for GC-376 PROTAC and of 4.6 μM for GC-376 PROTAC precursor (Figure S6). Such values proved to be in line with those displayed with respect to parent SARS-CoV-2 3CL^{Pro} (21.2 and 1.35 μM, respectively) [12], still supporting similar molecular recognition in the active site of both enzymes.

A

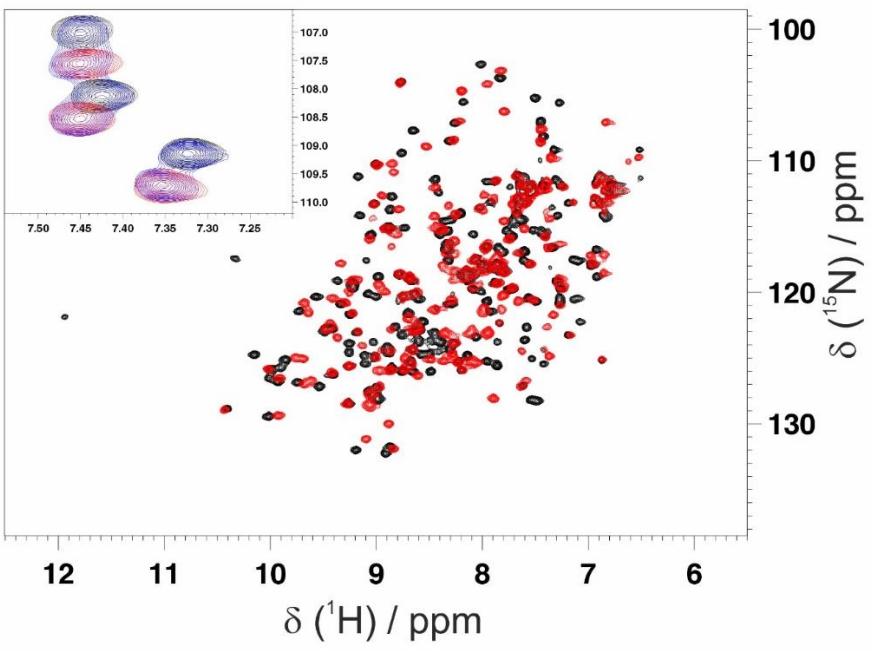

B

 doi:10.20944/preprints202407.1449.v1

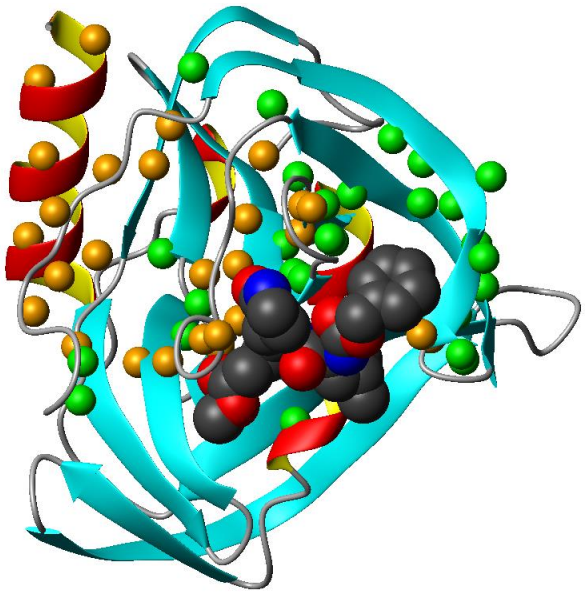

Figure 3. Mapping the interaction between GC-376 PROTAC precursor and CVB3 $3C^{Pro}$ by solution NMR. (**A**) Overlay of the ^{1}H-^{15}N HSQC spectra of CVB3 $3C^{Pro}$ before (red) and after (black) the addition of 1 equivalent of GC-376 PROTAC precursor recorded at 308K. In the inset, three NH signals in a slow exchange regime of the NMR time scale were shown at 0 (red), 0.5 (blue) and 1 (black) equivalents of GC-376 PROTAC precursor additions. (**B**) The backbone NHs showing chemical shifts changes larger than the threshold value, obtained by Figure S4, are mapped as green spheres on the crystal structure of CVB3 $3C^{Pro}$ complexed with GC-376 PROTAC precursor. The backbone NHs, unassigned in the CVB3 $3C^{Pro}$ and displaying increasing intensities along the stepwise additions of the GC-376 PROTAC precursor with their chemical shifts corresponding to those of the GC-376 PROTAC precursor-bound species, are shown as orange spheres.

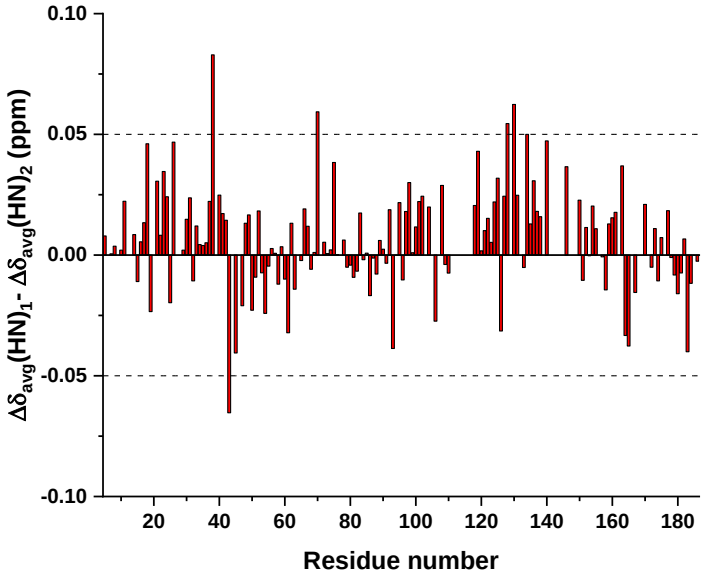

Figure 4. Monitoring the interaction of GC-376 PROTAC with CVB3 $3C^{Pro}$ by solution NMR. Subtraction of the backbone weighted average chemical shift differences ($\Delta\delta_{avg}$(HN)) obtained between ^{15}N-labelled CVB3 $3C^{Pro}$ and its 1:1 mixture with GC-376 PROTAC precursor $(\Delta\delta_{avg}(HN))_1$ and between ^{15}N-labelled CVB3 $3C^{Pro}$ and its 1:1 mixture with GC-376 PROTAC $(\Delta\delta_{avg}(HN))_2$.

 doi:10.20944/preprints202407.1449.v1

4. Discussion

The conservation of the main protease in viral genomes and the fact that humans do not have a homologous protease make this enzyme family an ideal target to develop broad-spectrum antiviral drugs with no toxicity against the host cell. These features have driven to the development of several classes of viral inhibitors able to block the function of this target. Among them, GC-376 is one of the most efficient 3CL protease inhibitors found to inhibit the activity of coronavirus $3CL^{Pro}$ [54]. A recent study showed that GC-376 is a potent 3CL protease inhibitor that binds with different kinds of coronavirus $3CL^{Pro}$ and a variety of $3CL^{Pro}$ mutants of SARS-CoV-2 to exert inhibitory activity [55]. In particular, GC-376 was shown to have a strong inhibitory activity against three pathogenic coronaviruses, i.e. SARS-CoV, MERS-CoV and SARS-CoV-2 $3CL^{Pro}$s. Recently, we have shown that a GC-376 based peptidomimetic PROTAC specifically targets and degrades the dimeric SARS-CoV-2 $3CL^{Pro}$ protein [12]. Several other PROTACs have been recently described to perform this function against both α- and β-groups of coronaviruses [11,13,14,56]. Here, we have extended the application of our GC-376 based peptidomimetic PROTAC to $3C^{Pro}$ protease, which is present in some members of the large genus Enterovirus. Specifically, we structurally characterized the interaction of the GC-376 PROTAC with CVB3 $3C^{Pro}$, a member of the enteroviral proteases, and we found that the GC-376 PROTAC interacts similarly to what found with SARS-CoV-2 $3CL^{Pro}$. The CG-376 moiety penetrates in the substrate binding site while the linker and the pomalidomide moiety are not tightly bound to CVB3 $3C^{Pro}$ but remain exposed to the solvent. The binding of CG-376 moiety in CVB3 $3C^{Pro}$ is similar to its binding in SARS-CoV-2 $3CL^{Pro}$, but there are some notable differences. The main difference lies in the orientation of the phenylmethyl ester of the CG-376 moiety, which is significantly altered between the two structures. This difference is also observed when the CG-376 inhibitor binds to $3CL^{Pro}$ of SARS-CoV-2, SARS-CoV and MERS-CoV [55]. In these crystal structures, the phenylmethyl ester is indeed not immobilized but it displays two conformations: “cis” and “trans”. In Figure 5A and 5C, the trans conformation of the phenylmethyl ester of the GC-376 precursor bound to $3CL^{Pro}$ of SARS-CoV-2 can be observed. While a cis conformation occurs for the phenylmethyl ester of the GC-376 precursor bound to CVB3 $3C^{Pro}$ (Figure 5A,D). This cis/trans conformational feature is therefore common to both $3C^{Pro}$ and $3CL^{Pro}$ proteases, indicating that the S4 subsite of the substrate cavity is an open space where the phenylmethyl ester of GC-376 can extend to the solvent and it is relatively flexible due to limited stabilizing forces. Other minor structural differences include the ligand interactions with subsites S1 and S2. The isobutyl group, which inserts into the S2 subsite of both proteases, shows hydrophobic interactions with multiple hydrophobic amino acid residues in $3CL^{Pro}$ structure of SARS-CoV-2, stabilizing its binding to S2 site (Figure 5A). This hydrophobic patch is not fully maintained in CVB3 $3C^{Pro}$ structure. Indeed, the catalytic Glu71, which is absent in coronaviral $3CL^{Pro}$s, is located with its negative charge next to the isobutyl group (Figure 5B). Finally, the γ-lactam ring of GC-376, which inserts into the S1 subsite of both proteases, while it forms similar interactions with the catalytic Cys and His161/163, conserved in both $3C^{Pro}$ and $3CL^{Pro}$ proteases, it has other different surrounding residues in the two proteases. Specifically, there are several residues located in the same structural positions of the S1 subsite of both proteases that are exchanged: Phe140→Thr142, Asn142→Ala144, Ser144→Gln146 and Glu166→Gly163,164,166 (Figure 5C,D). Overall, we can conclude that, although a considerable sequence diversity in the substrate binding sites of $3C^{Pro}$ and $3CL^{Pro}$, the GC-376 PROTAC can accommodate well in the binding sites of both proteases, demonstrating its potential applicability as a broad-spectrum antiviral PROTAC.

 doi:10.20944/preprints202407.1449.v1

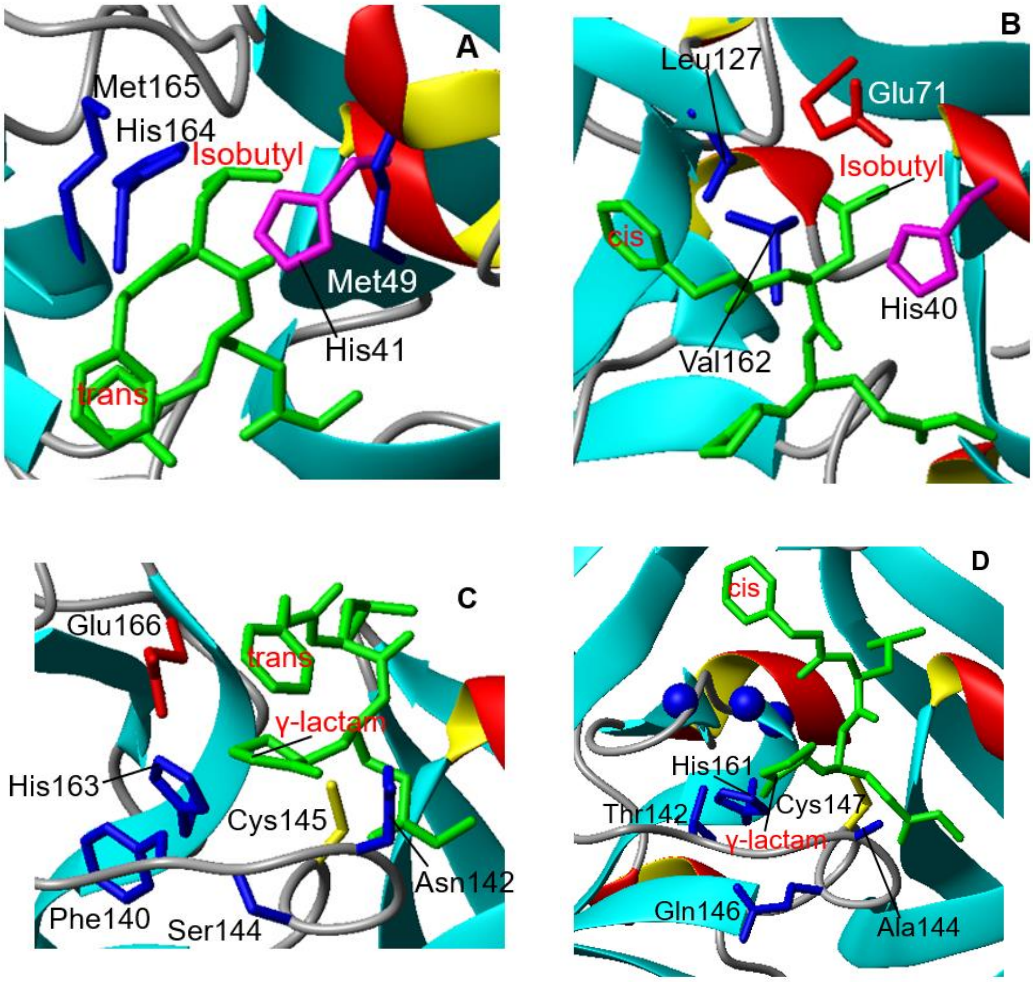

Figure 5. Structural comparison of the ligand-protein interactions occurring in subsites S1 and S2 of CVB3 $3C^{Pro}$ and SARS-CoV-2 $3CL^{Pro}$. (**A**) The side-chains of the hydrophobic residues surrounding the isobutyl group of the GC-376 precursor (in green) are shown in blue on the SARS-CoV-2 $3CL^{Pro}$ structure. The side-chain of the catalytic His41 is shown in magenta. The trans conformation of phenylmethyl ester is indicated. (**B**) The side-chains of the hydrophobic residues surrounding the isobutyl group of the GC-376 precursor (in green) are shown in blue on the CVB3 $3C^{Pro}$ structure. The side-chains of the catalytic His40 and Glu71 are shown in magenta and red, respectively. The cis conformation of phenylmethyl ester is indicated. (**C**) The side-chains of the residues surrounding the γ-lactam ring of the GC-376 precursor (in green) are shown in blue or red (for Glu166) on the SARS-CoV-2 $3CL^{Pro}$ structure. The side-chain of the catalytic Cys145 is shown in yellow. (**D**) The side-chains of the residues surrounding the γ-lactam ring of the GC-376 precursor (in green) are shown in blue on the CVB3 $3C^{Pro}$ structure. The backbone nitrogen atom of Gly163,164,166 are shown as blue spheres. The side-chain of the catalytic Cys147 is shown in yellow.

Supplementary Materials: Table S1, Data collection and refinement statistics of the crystal structure of CVB3 $3C^{Pro}$ in complex with GC-376 PROTAC precursor; Figure S1, Chemical formula of GC-376 PROTAC precursor and GC-376 PROTAC; Figure S2, Purification and protein size of CVB3 $3C^{Pro}$; Figure S3, Solution NMR spectra of CVB3 $3C^{Pro}$ at 298K; Figure S4, ^{15}N relaxation data of CVB3 $3C^{Pro}$; Figure S5, Mapping the interaction between GC-376 PROTAC precursor and CVB3 $3C^{Pro}$ by solution NMR; Figure S6. Inhibition curves of GC-376 PROTAC and of the corresponding precursor.

Author Contributions: Conceptualization, S.C.-B., V.C. and F.C.; Formal analysis, V.C., A.T. and D.G.; Funding acquisition, A.R., M.D. and S.C.-B.; Investigation, A.D.S., A.O. and E.L.; Project administration, A.R. and F.C.; Resources, D.G.; Supervision, F.C. and V.C.; Visualization, A.D.S. and D.G.; Writing - original draft, S.C.-B., F.C. and V.C.; Writing - review & editing, All Authors. All authors have read and agreed to the published version of the manuscript.

 doi:10.20944/preprints202407.1449.v1

Funding: This research was funded by "Fondo di beneficienza ed opere di carattere sociale e culturale" of Intesa Sanpaolo (project number B/2021/0212), by "the European Union-NextGenerationEU-National Recovery and Resilience Plan, Mission 4 Component 2-Investment 1.5-THE-Tuscany Health Ecosystem-ECS00000017-CUP B83C22003920001, and by the National Recovery and Resilience Plan, Mission 4, Component 2, Investment 1.1, Call for tender No. 104 published on 2.2.2022 by the Italian Ministry of University and Research (MUR), funded by the European Union – NextGenerationEU– Project Title "PROTAC-based approach to develop broad-spectrum antiviral drugs triggering the proteolysis of the main viral protease" – CUP B53D23015510006 - Grant Assignment Decree No. 1064 adopted on July 18th, 2023 by the Italian Ministry of Ministry of University and Research (MUR).

Institutional Review Board Statement: Not applicable.

Informed Consent Statement: Not applicable.

Data Availability Statement: **C**oordinates and structure factors have been deposited at the PDB under the accession code 8S6F for CVB3 3CPro complexed with GC-376 PROTAC precursor. The backbone resonance assignment of the GC-376 PROTAC precursor-bound state of CVB3 $3C^{Pro}$ at 308 K has been deposited in the BioMagResBank (BMRB ID 52547).

Acknowledgments: This publication was supported by the European Virus Archive Global (EVA-GLOBAL) project that has received funding from the European Union's Horizon 2020 research andinnovation programme under grant agreement No 871029. S.C.B. acknowledges support from COST Action, FeSImmChemNet. This article is based upon work from COST Action FeSImmChemNet, CA21115, supported by COST (European Cooperation in Science and Technology). F.C and V.C. acknowledge the support of the Italian Ministry of University and Research (MUR) through Dipartimenti di Eccellenza 2023-2027 (DICUS 2.0) to the Department of Chemistry "Ugo Schiff" of the University of Florence.

Conflicts of Interest: The authors declare no conflict of interest.

References

1. Komander, D.; Rape, M. The ubiquitin code. *Annu Rev Biochem* **2012**, *81*, 203-229.
2. Zheng, N.; Shabek, N. Ubiquitin Ligases: Structure, Function, and Regulation. *Annu Rev Biochem* **2017**, *86*, 129-157.
3. Morreale, F.E.; Walden, H. Types of Ubiquitin Ligases. *Cell* **2016**, *165*, 248-248.e241.
4. Deshaies, R.J.; Joazeiro, C.A. RING domain E3 ubiquitin ligases. *Annu Rev Biochem* **2009**, *78*, 399-434.
5. Schulman, B.A.; Harper, J.W. Ubiquitin-like protein activation by E1 enzymes: the apex for downstream signalling pathways. *Nat Rev Mol Cell Biol* **2009**, *10*, 319-331.
6. Ye, Y.; Rape, M. Building ubiquitin chains: E2 enzymes at work. *Nat Rev Mol Cell Biol* **2009**, *10*, 755-764.
7. Finley, D. Recognition and processing of ubiquitin-protein conjugates by the proteasome. *Annu. Rev. Biochem* **2009**, *78*, 477-513.
8. Li, K.; Crews, C.M. PROTACs: past, present and future. *Chem Soc Rev* **2022**, *51*, 5214-5236.
9. Ciulli, A.H., O. PROTAC Degraders Mechanism, Recent Advances, and Future Challenges. In *Protein Homeostasis in Drug Discovery: A Chemical Biology Perspective*, Jones, M.K.L.H., Ed. John Wiley & Sons, Inc.: 2022; pp. 317-356.
10. Toure, M.; Crews, C.M. Small-Molecule PROTACS: New Approaches to Protein Degradation. *Angew Chem Int Ed Engl* **2016**, *55*, 1966-1973.
11. Alugubelli, Y.R.; Xiao, J.; Khatua, K.; Kumar, S.; Sun, L.; Ma, Y.; Ma, X.R.; Vulupala, V.R.; Atla, S.; Blankenship, L.R., et al. Discovery of First-in-Class PROTAC Degraders of SARS-CoV-2 Main Protease. *J Med Chem* **2024**, *67*, 6495-6507.
12. Grifagni, D.; Lenci, E.; De Santis, A.; Orsetti, A.; Barracchia, C.G.; Tedesco, F.; Bellini Puglielli, R.; Lucarelli, F.; Lauriola, A.; Assfalg, M., et al. Development of a GC-376 Based Peptidomimetic PROTAC as a Degrader of 3-Chymotrypsin-like Protease of SARS-CoV-2. *ACS Med Chem Lett* **2024**, *15*, 250-257.
13. Desantis, J.; Bazzacco, A.; Eleuteri, M.; Tuci, S.; Bianconi, E.; Macchiarulo, A.; Mercorelli, B.; Loregian, A.; Goracci, L. Design, synthesis, and biological evaluation of first-in-class indomethacin-based PROTACs degrading SARS-CoV-2 main protease and with broad-spectrum antiviral activity. *European journal of medicinal chemistry* **2024**, *268*, 116202.
14. Sang, X.; Wang, J.; Zhou, J.; Xu, Y.; An, J.; Warshel, A.; Huang, Z. A Chemical Strategy for the Degradation of the Main Protease of SARS-CoV-2 in Cells. *J. Am. Chem. Soc.* **2023**, *145*, 27248-27253.

15. Anand, K.; Ziebuhr, J.; Wadhwani, P.; Mesters, J.R.; Hilgenfeld, R. Coronavirus main proteinase (3CLpro) structure: basis for design of anti-SARS drugs. *Science* **2003**, *300*, 1763-1767.
16. Marjomäki, V.; Kalander, K.; Hellman, M.; Permi, P. Enteroviruses and coronaviruses: similarities and therapeutic targets. *Expert opinion on therapeutic targets* **2021**, *25*, 479-489.
17. Wen, W.; Qi, Z.; Wang, J. The Function and Mechanism of Enterovirus 71 (EV71) 3C Protease. *Current microbiology* **2020**, *77*, 1968-1975.
18. Laitinen, O.H.; Svedin, E.; Kapell, S.; Nurminen, A.; Hytönen, V.P.; Flodström-Tullberg, M. Enteroviral proteases: structure, host interactions and pathogenicity. *Reviews in medical virology* **2016**, *26*, 251-267.
19. Tan, J.; George, S.; Kusov, Y.; Perbandt, M.; Anemüller, S.; Mesters, J.R.; Norder, H.; Coutard, B.; Lacroix, C.; Leyssen, P., et al. 3C protease of enterovirus 68: structure-based design of Michael acceptor inhibitors and their broad-spectrum antiviral effects against picornaviruses. *J Virol* **2013**, *87*, 4339-4351.
20. Nikonov, O.S.; Chernykh, E.S.; Garber, M.B.; Nikonova, E.Y. Enteroviruses: Classification, Diseases They Cause, and Approaches to Development of Antiviral Drugs. *Biochemistry. Biokhimiia* **2017**, *82*, 1615-1631.
21. Maier, R.; Krebs, P.; Ludewig, B. Immunopathological basis of virus-induced myocarditis. *Clinical & developmental immunology* **2004**, *11*, 1-5.
22. Gauntt, C.; Huber, S. Coxsackievirus experimental heart diseases. *Front Biosci* **2003**, *8*, e23-35.
23. Lugo, D.; Krogstad, P. Enteroviruses in the early 21st century: new manifestations and challenges. *Current opinion in pediatrics* **2016**, *28*, 107-113.
24. Fan, W.; McDougal, M.B.; Schoggins, J.W. Enterovirus 3C Protease Cleaves TRIM7 To Dampen Its Antiviral Activity. *J Virol* **2022**, *96*, e0133222.
25. Gorbalenya, A.E.; Donchenko, A.P.; Blinov, V.M.; Koonin, E.V. Cysteine proteases of positive strand RNA viruses and chymotrypsin-like serine proteases. A distinct protein superfamily with a common structural fold. *FEBS Lett* **1989**, *243*, 103-114.
26. Fan, K.; Wei, P.; Feng, Q.; Chen, S.; Huang, C.; Ma, L.; Lai, B.; Pei, J.; Liu, Y.; Chen, J., et al. Biosynthesis, purification, and substrate specificity of severe acute respiratory syndrome coronavirus 3C-like proteinase. *J Biol Chem* **2004**, *279*, 1637-1642.
27. Zhang, L.; Lin, D.; Kusov, Y.; Nian, Y.; Ma, Q.; Wang, J.; von Brunn, A.; Leyssen, P.; Lanko, K.; Neyts, J., et al. α-Ketoamides as Broad-Spectrum Inhibitors of Coronavirus and Enterovirus Replication: Structure-Based Design, Synthesis, and Activity Assessment. *J Med Chem* **2020**, *63*, 4562-4578.
28. Anand, K.; Palm, G.J.; Mesters, J.R.; Siddell, S.G.; Ziebuhr, J.; Hilgenfeld, R. Structure of coronavirus main proteinase reveals combination of a chymotrypsin fold with an extra alpha-helical domain. *Embo j* **2002**, *21*, 3213-3224.
29. Fàbrega-Ferrer, M.; Herrera-Morandé, A.; Muriel-Goñi, S.; Pérez-Saavedra, J.; Bueno, P.; Castro, V.; Garaigorta, U.; Gastaminza, P.; Coll, M. Structure and inhibition of SARS-CoV-1 and SARS-CoV-2 main proteases by oral antiviral compound AG7404. *Antiviral research* **2022**, *208*, 105458.
30. Göhl, M.; Zhang, L.; El Kilani, H.; Sun, X.; Zhang, K.; Brönstrup, M.; Hilgenfeld, R. From Repurposing to Redesign: Optimization of Boceprevir to Highly Potent Inhibitors of the SARS-CoV-2 Main Protease. *Molecules* **2022**, *27*.
31. Lockbaum, G.J.; Henes, M.; Lee, J.M.; Timm, J.; Nalivaika, E.A.; Thompson, P.R.; Kurt Yilmaz, N.; Schiffer, C.A. Pan-3C Protease Inhibitor Rupintrivir Binds SARS-CoV-2 Main Protease in a Unique Binding Mode. *Biochemistry* **2021**, *60*, 2925-2931.
32. Dai, W.; Jochmans, D.; Xie, H.; Yang, H.; Li, J.; Su, H.; Chang, D.; Wang, J.; Peng, J.; Zhu, L., et al. Design, Synthesis, and Biological Evaluation of Peptidomimetic Aldehydes as Broad-Spectrum Inhibitors against Enterovirus and SARS-CoV-2. *J Med Chem* **2022**, *65*, 2794-2808.
33. Ramajayam, R.; Tan, K.P.; Liu, H.G.; Liang, P.H. Synthesis and evaluation of pyrazolone compounds as SARS-coronavirus 3C-like protease inhibitors. *Bioorg Med Chem* **2010**, *18*, 7849-7854.
34. Ramajayam, R.; Tan, K.P.; Liang, P.H. Recent development of 3C and 3CL protease inhibitors for anti-coronavirus and anti-picornavirus drug discovery. *Biochem Soc Trans* **2011**, *39*, 1371-1375.
35. Mandadapu, S.R.; Weerawarna, P.M.; Prior, A.M.; Uy, R.A.; Aravapalli, S.; Alliston, K.R.; Lushington, G.H.; Kim, Y.; Hua, D.H.; Chang, K.O., et al. Macrocyclic inhibitors of 3C and 3C-like proteases of picornavirus, norovirus, and coronavirus. *Bioorg Med Chem Lett* **2013**, *23*, 3709-3712.
36. Kumar, V.; Shin, J.S.; Shie, J.J.; Ku, K.B.; Kim, C.; Go, Y.Y.; Huang, K.F.; Kim, M.; Liang, P.H. Identification and evaluation of potent Middle East respiratory syndrome coronavirus (MERS-CoV) 3CL(Pro) inhibitors. *Antiviral research* **2017**, *141*, 101-106.

37. Lee, C.C.; Kuo, C.J.; Ko, T.P.; Hsu, M.F.; Tsui, Y.C.; Chang, S.C.; Yang, S.; Chen, S.J.; Chen, H.C.; Hsu, M.C., et al. Structural basis of inhibition specificities of 3C and 3C-like proteases by zinc-coordinating and peptidomimetic compounds. *J Biol Chem* **2009**, *284*, 7646-7655.
38. Kuo, C.J.; Liu, H.G.; Lo, Y.K.; Seong, C.M.; Lee, K.I.; Jung, Y.S.; Liang, P.H. Individual and common inhibitors of coronavirus and picornavirus main proteases. *FEBS Lett* **2009**, *583*, 549-555.
39. Fili, S.; Valmas, A.; Christopoulou, M.; Spiliopoulou, M.; Nikolopoulos, N.; Lichière, J.; Logotheti, S.; Karavassili, F.; Rosmaraki, E.; Fitch, A., et al. Coxsackievirus B3 protease 3C: expression, purification, crystallization and preliminary structural insights. *Acta crystallographica. Section F, Structural biology communications* **2016**, *72*, 877-884.
40. Kabsch, W. XDS. *Acta Crystallogr. D. Biol. Crystallogr* **2010**, *66*, 125-132.
41. Vagin, A.A.; Teplyakov, A. An approach to multi-copy search in molecular replacement. *Acta Cryst. D* **2000**, *56*, 1622-1624.
42. Adams, P.D.; Afonine, P.V.; Bunkoczi, G.; Chen, V.B.; Davis, I.W.; Echols, N.; Headd, J.J.; Hung, L.W.; Kapral, G.J.; Grosse-Kunstleve, R.W., et al. PHENIX: a comprehensive Python-based system for macromolecular structure solution. *Acta Crystallogr. D. Biol. Crystallogr* **2010**, *66*.
43. Emsley, P.; Lohkamp, B.; Scott, W.G.; Cowtan, K. Features and development of Coot. *Acta Cryst. D* **2010**, *66*, 486-501.
44. Chen, V.B.; Arendall, W.B., III.; Headd, J.J.; Keedy, D.A.; Immormino, R.M.; Kapral, G.J.; Murray, L.W.; Richardson, J.S.; Richardson, D.C. MolProbity: all-atom structure validation for macromolecular crystallography. *Acta Cryst. D* **2010**, *66*, 12-21.
45. Grzesiek, S.; Bax, A. Amino acid type determination in the sequential assignment procedure of uniformly 13C/15N-enriched proteins. *J. Biomol. NMR* **1993**, *3*, 185-204.
46. Williamson, M.P. Using chemical shift perturbation to characterise ligand binding. *Prog. Nucl. Magn Reson. Spectrosc* **2013**, *73*, 1-16.
47. Farrow, N.A.; Muhandiram, R.; Singer, A.U.; Pascal, S.M.; Kay, C.M.; Gish, G.; Shoelson, S.E.; Pawson, T.; Forman-Kay, J.D.; Kay, L.E. Backbone dynamics of a free and phosphopeptide-complexed Src homology 2 domain studied by 15N NMR relaxation. *Biochemistry* **1994**, *33*, 5984-6003.
48. Grzesiek, S.; Bax, A. The Importance of Not Saturating H2o in Protein Nmr - Application to Sensitivity Enhancement and Noe Measurements. *J. Am. Chem. Soc.* **1993**, *115*, 12593-12594.
49. Mandel, M.A.; Akke, M.; Palmer, A.G., III. Backbone dynamics of *Escherichia coli* ribonuclease HI: correlations with structure and function in an active enzyme. *J. Mol. Biol* **1995**, *246*, 144-163.
50. Garcia de la Torre, J.; Huertas, M.L.; Carrasco, B. HYDRONMR: prediction of NMR relaxation of globular proteins from atomic-level structures and hydrodynamic calculations. *J Magn Reson* **2000**, *147*, 138-146.
51. Matthews, D.A.; Dragovich, P.S.; Webber, S.E.; Fuhrman, S.A.; Patick, A.K.; Zalman, L.S.; Hendrickson, T.F.; Love, R.A.; Prins, T.J.; Marakovits, J.T., et al. Structure-assisted design of mechanism-based irreversible inhibitors of human rhinovirus 3C protease with potent antiviral activity against multiple rhinovirus serotypes. *Proc Natl Acad Sci U S A* **1999**, *96*, 11000-11007.
52. Johnson, T.O.; Hua, Y.; Luu, H.T.; Brown, E.L.; Chan, F.; Chu, S.S.; Dragovich, P.S.; Eastman, B.W.; Ferre, R.A.; Fuhrman, S.A., et al. Structure-based design of a parallel synthetic array directed toward the discovery of irreversible inhibitors of human rhinovirus 3C protease. *J Med Chem* **2002**, *45*, 2016-2023.
53. Golovanov, A.P.; Hautbergue, G.M.; Wilson, S.A.; Lian, L.Y. A simple method for improving protein solubility and long-term stability. *J. Am. Chem. Soc* **2004**, *126*, 8933-8939.
54. Fu, L.; Ye, F.; Feng, Y.; Yu, F.; Wang, Q.; Wu, Y.; Zhao, C.; Sun, H.; Huang, B.; Niu, P., et al. Both Boceprevir and GC376 efficaciously inhibit SARS-CoV-2 by targeting its main protease. *Nat Commun* **2020**, *11*, 4417.
55. Lin, C.; Zhu, Z.; Jiang, H.; Zou, X.; Zeng, X.; Wang, J.; Zeng, P.; Li, W.; Zhou, X.; Zhang, J., et al. Structural Basis for Coronaviral Main Proteases Inhibition by the 3CLpro Inhibitor GC376. *J Mol Biol* **2024**, *436*, 168474.
56. Cheng, S.; Feng, Y.; Li, W.; Liu, T.; Lv, X.; Tong, X.; Xi, G.; Ye, X.; Li, X. Development of novel antivrial agents that induce the degradation of the main protease of human-infecting coronaviruses. *European journal of medicinal chemistry* **2024**, *275*, 116629.